

Rapidity-Dependent Spin Decomposition of the Nucleon

Florian Hechenberger,^{1,*} Kiminad A. Mamo,^{2,†} and Ismail Zahed^{1,‡}

¹*Center for Nuclear Theory, Stony Brook University, Stony Brook, NY 11794, USA*

²*Department of Physics, William & Mary, Williamsburg, VA 23187, USA*

(Dated: July 25, 2025)

We show that the two-dimensional Fourier transform of the generalized parton distributions (GPDs) has *two* distinct interpretations: at zero skewness ($\eta = 0$) it yields the familiar impact-parameter density, while at finite skewness ($\eta \neq 0$) it encodes a genuine *parton–nucleon correlation* whose norm decreases predictably with the rapidity gap $\Delta y = 2 \operatorname{artanh} \eta$. This rapidity dependence produces universal *rapidity-modified Ji identities* linking helicity, orbital, and total angular momenta analytically. Using linear open- and closed-string Regge trajectories constrained by empirical PDFs, spectroscopy and form factor data, we obtain the leading-twist GPDs H, E, \tilde{H} across the full (x, η, t) range. Numerical Mellin–Barnes inversion agrees with existing lattice data and yields rapidity-resolved predictions for Jefferson Lab 12 GeV, the Electron–Ion Collider, and forthcoming lattice studies.

Introduction.— Generalized parton distributions (GPDs) extend ordinary parton densities by correlating the longitudinal momentum fraction x , the transverse position \mathbf{b}_\perp , and the spin of quarks and gluons in a single Lorentz-covariant object [1–7]. They can be regarded as elementary form factors of partons in luminal hadrons. They enter hard exclusive processes such as deeply-virtual Compton scattering (DVCS) and meson production, offering simultaneous sensitivity to the nucleon’s three-dimensional spatial and momentum structure. They are essential for our understanding of the origin of spin and mass in hadrons, and in a way in most of the visible mass in the universe. Extracting this information has become a central goal of Jefferson Lab and the future Electron–Ion Collider (EIC) [8, 9].

At *zero* longitudinal momentum transfer ($\eta = 0$) the two-dimensional Fourier transform of an unpolarized GPD

$$\rho(x, b_\perp) = \int \frac{d^2 \Delta_\perp}{(2\pi)^2} e^{-i\Delta_\perp \cdot \mathbf{b}_\perp} H(x, \eta=0, -\Delta_\perp^2),$$

has a genuine probability interpretation: it is the density of partons carrying fraction x of the proton’s plus momentum and located at transverse position \mathbf{b}_\perp relative to the proton’s center [10, 11]. The probability interpretation, however, hinges critically on $\eta = 0$.

For non-zero longitudinal momentum transfer ($\eta \neq 0$) the impact-parameter amplitude $\rho(b_\perp, \eta)$ loses its probabilistic meaning. It now represents an *off-diagonal* matrix element—a true quantum correlation between the incoming and outgoing nucleon—generated by gauge-invariant light-ray operators [7, 12].

For instance, a quark light ray describes a quark being removed from the proton with longitudinal momentum fraction $x + \eta$, and being put back with momentum fraction $x - \eta$ at a given transverse separation b_\perp .

In the present framework, which is based on [13, 14], that probe is modeled explicitly by linear *open* (colorless quark-pair) and *closed* (colorless gluon-pair) string

trajectories: the open or closed string in the t -channel, probes the nucleon, with the latter re-emerging with a shifted longitudinal momentum, or rapidity gap $\Delta y = 2 \operatorname{artanh}(\eta)$. The Hankel kernel of the 2D Fourier transform therefore measures how strongly these "string quanta" (colorless parton-pairs) correlate with the nucleon at a transverse separation b_\perp for a given skewness η or rapidity gap Δy . At $\eta = 0$ the overlap reduces to a diagonal (probabilistic) density, while at $\eta \neq 0$ it encodes the full rapidity-dependent off-forward structure that is central to the stringy GPD parametrization first developed in [13, 14].

This reinterpretation has several consequences. First, the familiar Ji relations [15] now quantify the *effective* spin, helicity and orbital content of the parton–nucleon correlation rather than of the proton alone. Because the norm of that correlation changes with η , all contributions to the standard spin sum rule acquire explicit skewness-dependent prefactors that track how helicity and orbital components of the t -channel colorless parton-pairs redistribute as the rapidity gap grows. Second, global DVCS analyses—whose inverse kernels couple directly to conformal moments—must include these prefactors once precise finite-skewness data from Jefferson Lab 12 GeV and the EIC become available (see [16] for the exact mapping between conformal moments and Compton form factors of DVCS). Third, lattice calculations performed at non-zero momentum transfer can confront our predictions at finite skewness, providing a stringent check on both quark and gluon operator probes.

Conformal moments.— Our construction starts from the Mellin–Barnes (MB) representation of leading-twist quark ($a = q$) and gluon ($a = g$) GPDs,

$$F_a(x, \eta, t; \mu) = \frac{s_a}{2i} \int_{c-i\infty}^{c+i\infty} \frac{dj}{\sin(\pi j)} p_a(j, x, \eta) \mathbb{F}_a(j, \eta, t; \mu), \quad (1)$$

where $s_q = 1$ and $s_g = -1$ is a pertinent sign reflecting on the particle’s symmetry. Here the partial waves

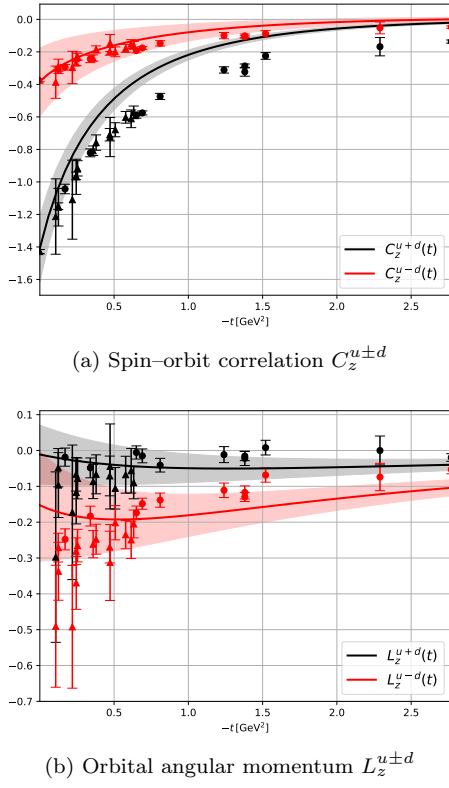


FIG. 1: Isoscalar spin-orbit correlation and quark orbital angular momentum in the nucleon versus $-t$ at $\mu = 2$ GeV. Bands: this work; circles: [18]; triangles: LHPC [19].

(PWs) $p_a(j, x, \eta)$ are the analytically continued Gegenbauer kernels both in the ERBL ($-\eta \leq x \leq \eta$) and DGLAP ($x \geq \eta$) regimes [17]. The constant c is chosen such that the sums in the conformal partial wave expansion are correctly reproduced, see [13] for the explicit expressions of the PWs, and the flavor decompositions. All dynamical information is therefore encoded in the *conformal moments* $\mathbb{F}_a(j, \eta, t; \mu)$, analytic in the complex spin j .

Gauge/string duality predicts that, at fixed $|t|$ and large partonic center-of-mass energy, the t -channel is dominated by *linear* open- (colorless quark-pair) and closed-string (colorless gluon-pair) trajectories [22, 23]. For vanishing skewness ($\eta = 0$) we thus model the conformal moments at the hadronic scale $\mu_0 = 1$ GeV by the “Reggeized” Mellin transform

$$\mathcal{F}_a(j, t) \equiv \mathbb{F}_a(j, 0, t; \mu_0) = \int_0^1 dx \frac{f_a(x, \mu_0)}{x^{j-1+\alpha'_a t}}. \quad (2)$$

The PDFs are fixed *once and for all* to MSTW09 NLO (unpolarized) [24] and AAC NLO (polarized) [25]. The Regge slopes α'_a are taken from hadron and glueball spectroscopy and form factors, see Table S1 in the **End Matter** for their numerical values. No additional parameters are introduced.

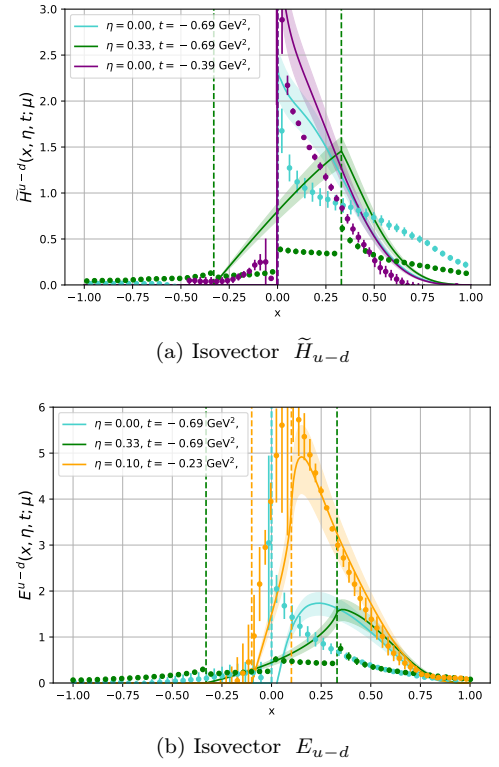


FIG. 2: String-Regge x -space nucleon non-singlet/(-) combination of GPDs reconstructed via Mellin-Barnes inversion for the isovector channel, and their comparison with lattice data [20, 21]. All curves are evolved to $\mu = 2$ GeV at NLO.

To obtain $\eta \neq 0$ one multiplies the forward moments by a unique hypergeometric kernel that enforces analyticity, crossing symmetry and removes spurious poles [13, 26]

$$\mathbb{F}_a(j, \eta, t; \mu_0) = [\hat{d}_j(\eta, t) - 1] [\mathcal{F}_a(j, t) - \mathcal{F}_a^S(j, t)] + \mathcal{F}_a(j, t), \quad (3)$$

with

$$\hat{d}_j(\eta, t) = {}_2F_1\left(\frac{1}{2} - j, -\frac{j}{2}; \frac{1}{2}; -\frac{4m_N^2 \eta^2}{t}\right), \quad (4)$$

where \mathcal{F}_a^S is obtained from (2) by the replacement $\alpha'_a \rightarrow \alpha_a^S$. All leading-twist singlet and non-singlet moments $\{\mathbb{H}, \mathbb{E}, \tilde{\mathbb{H}}\}$ are evolved from μ_0 to an arbitrary scale μ by solving the NLO DGLAP-ERBL equations *directly in conformal space*.

Figure 1 shows the isovector and isoscalar spin-orbit correlation $C_z^{u\pm d}(t)$ and the OAM $L_z^{u\pm d}(t)$ at $\mu = 2$ GeV and $\eta = 0$. The curves reproduce the lattice results [18, 19] within uncertainties. For the general relations between conformal moments and the various observables in Figure 1, and the MB integrals used to generate Figure 2, we refer to [13, 14]. Further detailed comparisons with the recent lattice GPDs data [27] will be carried out elsewhere.

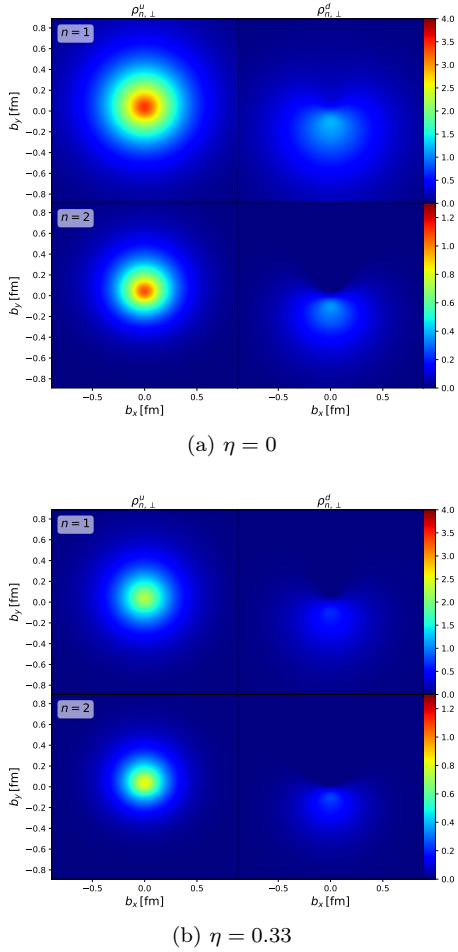


FIG. 3: Spatial tomography at $\mu = 2$ GeV showing the isovector and isoscalar non-singlet/($-$) combination quark transverse conformal moment densities $\rho_{n,\perp}^{u/d}(b_\perp, \eta)$ ($n = 1-2$) in the nucleon. Panel (a) is the zero-skewness case; panel (b) illustrates finite skewness $\eta = 0.33$ or rapidity gap $\Delta y = 0.69$.

The x -space GPDs at any (x, η, t) are recovered via numerical MB inversion of Eq. (1). Figure 2 (both panels) demonstrates that a *single* Regge parameter set reproduces fairly well the currently available lattice data for the non-singlet isovector sector. All error bars in this Letter’s figures reflect uncertainties propagated from the input PDFs.

Spatial tomography at arbitrary skewness.— For a proton polarized along $+\hat{y}$ the overlap between the colorless parton-pair probes and the recoiling nucleon is

$$\rho_n^{u\pm d}(\mathbf{b}_\perp; \eta) = \int \frac{d^2 \Delta_\perp}{(2\pi)^2} e^{-i\Delta_\perp \cdot \mathbf{b}_\perp} \left[\mathbb{H}_{u\pm d}^{(-)}(n, \eta, t) + i \frac{\Delta_y}{2m_N} \mathbb{E}_{u\pm d}^{(-)}(n, \eta, t) \right], \quad (5)$$

where $t = (-\Delta_\perp^2 - 4\eta^2 m_N^2)/(1 - \eta^2) \equiv -\left(\frac{\Delta_\perp^2}{1-\eta^2} + c_\eta\right)$

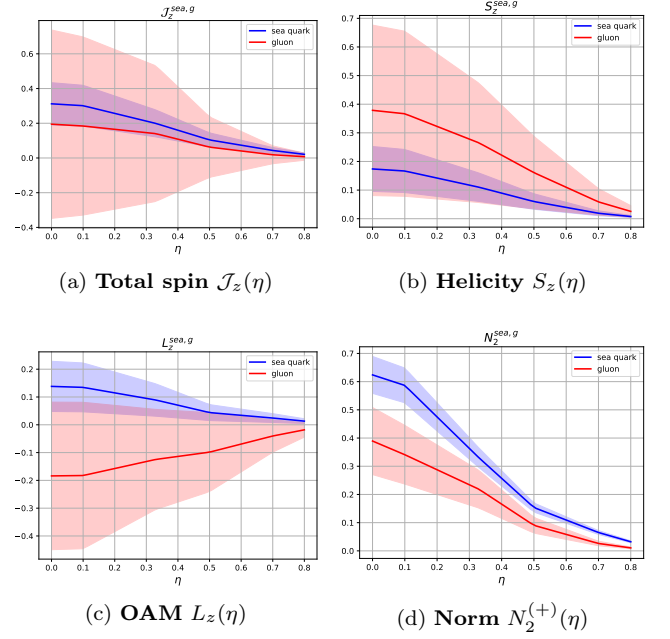


FIG. 4: Rapidity dependence of (a) the total spin, (b) helicity, (c) orbital angular momentum, and (d) overall norm of the parton–nucleon correlation at $\mu = 2$ GeV.

[7] with

$$c_\eta = 4\eta^2 m_N^2 / (1 - \eta^2). \quad (6)$$

Note that we have flavor separated the non-singlet ($-$) combination using $\rho_n^{u/d} = \frac{1}{2}(\rho_n^{u+d} \pm \rho_n^{u-d})$ as shown in Fig. 3. The overall strength of the parton–nucleon correlation is obtained by integrating the complete density (5) over the transverse plane,

$$N_n^{u\pm d}(\eta) = \int d^2 b_\perp \rho_n^{u\pm d}(\mathbf{b}_\perp; \eta) = \mathbb{H}_{u\pm d}^{(-)}(n, \eta, t = -c_\eta), \quad (7)$$

see **End Matter** for a derivation of (7). At $\eta = 0$ one recovers the familiar probabilistic normalization $N_n^{u\pm d}(0) = \mathbb{H}_{u\pm d}^{(-)}(n, 0, 0)$. Figure 3a shows the first two quark transverse moment densities at $\eta = 0$, showing that the large- b_\perp fall-off is controlled entirely by the Regge slopes in Table S1, without any additional fit parameters. Figure 3b shows the first two quark transverse moment densities at $\eta = 0.33$ (or $\Delta y = 0.69$) which is consistent with the decreasing of their norms with increasing skewness η (or increasing rapidity gap $\Delta y = 2 \operatorname{artanh}(\eta)$).

Spin tomography at arbitrary skewness.— For $\eta \neq 0$, the axial (\mathbb{H}_a) and vector ($\mathbb{H}_a, \mathbb{E}_a$) conformal moments govern, respectively, the helicity and total angular momentum carried by the parton–nucleon correlation. At $\eta = 0$ these moments satisfy Ji’s spin decomposition and sum rule as demonstrated in Table S2 which lists the resulting spin budget at $\eta = 0$. In the **End Matter**, we

have also shown the spin tomography in Fig. S1, which illustrates the helicity, OAM and spin-orbit densities at $\eta = 0$.

Because the total overlap strength or norm changes with skewness as shown in Eqs. (7), the effective helicity, orbital and total angular momentum of the parton-nucleon correlation at finite skewness $\eta \neq 0$ and $\Delta_{\perp} = 0$ read

$$S_z^a(\eta, -c_\eta) = \frac{1}{2} \widetilde{\mathbb{H}}_a^{(+)}(1, \eta, -c_\eta), \quad (8)$$

$$\begin{aligned} \mathcal{J}_z^a(\eta, -c_\eta) &= S_z^a(\eta, -c_\eta) + L_z^a(\eta, -c_\eta) \\ &= \frac{1}{2} [\mathbb{H}_a^{(+)}(2, \eta, -c_\eta) + \mathbb{E}_a^{(+)}(2, \eta, -c_\eta)], \quad (9) \end{aligned}$$

where $\mathbb{H}_a^{(+)}(2, \eta, -c_\eta) + \mathbb{E}_a^{(+)}(2, \eta, -c_\eta) \equiv A_a(-c_\eta)$ are just the spin-2 $A_a(t)$ gravitational form factors evaluated at $t = -c_\eta$ ¹. Note that the D-term contributions which are order of $\eta^2 D_a(t)$ are canceled between the unpolarized and helicity-flip form factors, and the $B_a(t)$ form factors are vanishing for the singlet [30]. Therefore, summing over flavors and gluons gives the *rapidity-modified Ji's identity*

$$\begin{aligned} \mathcal{J}_z(\eta) &= \sum_{a=q,g} [S_z^a(\eta, -c_\eta; \mu) + L_z^a(\eta, -c_\eta; \mu)] \\ &= \frac{1}{2} (A_q(-c_\eta) + A_g(-c_\eta)), \quad (10) \end{aligned}$$

where $\mathcal{J}_z(0) = \frac{1}{2}$ but decreases as the rapidity gap grows, reflecting the depletion of the parton-nucleon correlation. We have plotted $\mathcal{J}_z^a(\eta, -c_\eta)$, $S_z^a(\eta)$, $L_z^a(\eta)$, and $N_n^a(\eta)$ in Fig. 4. The error bands reflect mostly on the uncertainty of the input PDF parametrizations of Refs. [24, 25], which are propagated through the evolution equations, as all other numerical errors are negligible. Remarkably, in gauge/string duality, a similar depletion of the string mediated modes in lepton-hadron and hadron-hadron scattering is observed for large rapidity gaps in the Regge limit, a prelude to the onset of the universal Pomeron exchange [28, 31].

Conclusions.— We have introduced a fully analytic scheme in which linear open- and closed-string (or colorless quark- and gluon-pair) Regge trajectories act as universal probes of hadron structure. Empirical PDFs and form factors together with hadron and glueball spectroscopy fix every conformal moment, so the ensuing Mellin-Barnes inversion reconstructs H , E , and \tilde{H} for any (x, η, t) without adjustable parameters. The

framework reproduces all available lattice moments and x -space GPDs at $\eta = 0$, while at finite skewness it predicts genuine *parton-nucleon correlations* whose norm varies solely through the rapidity gap. This norm variation yields rapidity-modified Ji identities that quantitatively link helicity, orbital, and total angular momentum. The same formalism supplies prediction for sea-quark and gluon helicity moments and for transverse spin-orbit densities. Remarkably, the rapidity-dependent depletion of the parton-nucleon correlation we observe, closely parallels the depletion of string-mediated modes seen in gauge/string duality descriptions of high-energy Regge scattering [28, 31], suggesting a deep, universal connection between parton-nucleon spin correlations and Regge phenomenology. Because the approach is closed under QCD evolution, free of model tuning (other than the input PDFs and Regge slope parameters), and fast to evaluate, it can be used directly in upcoming global fits and lattice analyses, providing a self-consistent, rapidity-resolved picture of quark and gluon dynamics that is ready for Jefferson Lab 12 GeV and the future EIC.

OPEN DATA STATEMENT

To promote open and reproducible research, the computer code used to generate the numerical results and figures in this paper is available at <https://github.com/HechenMountain/stringy-gpds> and <https://zenodo.org/records/15738460>.

ACKNOWLEDGMENTS

We thank Martha Constantinou and Shunzo Kumano for discussions. F.H. is funded by the Austrian Science Fund (FWF) [10.55776/J4854]. For open access purposes, the author has applied a CC BY public copyright license to any author accepted manuscript version arising from this submission. F.H. also thanks Fabio Leimgruber for valuable assistance with code development and troubleshooting. K.M. is supported by DOE Grant No. DE-FG02-04ER41302 and by Contract No. DE-AC05-06OR23177 under which Jefferson Science Associates operates Jefferson Lab. I.Z. is supported by the U.S. Department of Energy under Grant No. DE-FG-88ER40388. This research forms part of the Quark-Gluon Tomography Topical Collaboration, Contract No. DE-SC0023646.

¹ In gauge/string duality, the gluonic gravitational form factor of the nucleon, maps onto the graviton-open-open string 3-vertex. In particular, the twist-2-spin-2 gluon operator $F^{\alpha\mu} F_\mu^\beta$ maps onto the massless graviton operator $h_{\alpha\beta} \partial X^\alpha \bar{\partial} X^\beta e^{ik \cdot X}$ on the disc worldsheet, and similarly for the twist-2-spin-j operators [28, 29]. The rapidity dependent parton-nucleon spin correlation noted here, reflects on the 3-vertex dependence on the rapidity gap.

* florian.hechenberger@stonybrook.edu

† kamamo@wm.edu

‡ ismail.zahed@stonybrook.edu

- [1] D. Müller, D. Robaschik, B. Geyer, F. M. Dittes, and J. Hořejši, *Fortsch. Phys.* **42**, 101 (1994), arXiv:hep-ph/9812448.
- [2] X.-D. Ji, *Phys. Rev. Lett.* **78**, 610 (1997), arXiv:hep-ph/9603249.
- [3] A. V. Radyushkin, *Phys. Lett. B* **380**, 417 (1996), arXiv:hep-ph/9604317.
- [4] A. V. Radyushkin, *Phys. Rev. D* **56**, 5524 (1997), arXiv:hep-ph/9704207.
- [5] X.-D. Ji and J. Osborne, *Phys. Rev. D* **58**, 094018 (1998), arXiv:hep-ph/9801260.
- [6] M. Diehl, *Phys. Rept.* **388**, 41 (2003), arXiv:hep-ph/0307382.
- [7] A. V. Belitsky and A. V. Radyushkin, *Phys. Rept.* **418**, 1 (2005), arXiv:hep-ph/0504030.
- [8] A. Accardi *et al.*, *Eur. Phys. J. A* **52**, 268 (2016), arXiv:1212.1701 [nucl-ex].
- [9] A. Accardi *et al.*, *Eur. Phys. J. A* **60**, 173 (2024), arXiv:2306.09360 [nucl-ex].
- [10] D. E. Soper, *Phys. Rev. D* **15**, 1141 (1977).
- [11] M. Burkardt, *Int. J. Mod. Phys. A* **18**, 173 (2003), arXiv:hep-ph/0207047.
- [12] M. Diehl, *Eur. Phys. J. C* **25**, 223 (2002), [Erratum: *Eur.Phys.J.C* 31, 277–278 (2003)], arXiv:hep-ph/0205208.
- [13] K. A. Mamo and I. Zahed, *Phys. Rev. Lett.* **133**, 241901 (2024), arXiv:2411.04162 [hep-ph].
- [14] K. A. Mamo and I. Zahed, *Phys. Rev. D* **110**, 114016 (2024), arXiv:2404.13245 [hep-ph].
- [15] X.-D. Ji, W. Melnitchouk, and X. Song, *Phys. Rev. D* **56**, 5511 (1997), arXiv:hep-ph/9702379.
- [16] K. Kumericki, S. Liuti, and H. Moutarde, *Eur. Phys. J. A* **52**, 157 (2016), arXiv:1602.02763 [hep-ph].
- [17] D. Mueller and A. Schafer, *Nucl. Phys. B* **739**, 1 (2006), arXiv:hep-ph/0509204.
- [18] S. Bhattacharya, K. Cichy, M. Constantinou, X. Gao, A. Metz, J. Miller, S. Mukherjee, P. Petreczky, F. Steffens, and Y. Zhao, *JHEP* **01**, 146, arXiv:2410.03539 [hep-lat].
- [19] P. Hagler *et al.* (LHPC), *Phys. Rev. D* **77**, 094502 (2008), arXiv:0705.4295 [hep-lat].
- [20] C. Alexandrou, K. Cichy, M. Constantinou, K. Hadjiyiannakou, K. Jansen, A. Scapellato, and F. Steffens, *Phys. Rev. Lett.* **125**, 262001 (2020), arXiv:2008.10573 [hep-lat].
- [21] J. Holligan and H.-W. Lin, *Phys. Rev. D* **110**, 034503 (2024), arXiv:2312.10829 [hep-lat].
- [22] R. C. Brower, J. Polchinski, M. J. Strassler, and C.-I. Tan, *JHEP* **12**, 005, arXiv:hep-th/0603115.
- [23] R. C. Brower, M. Djuric, and C.-I. Tan, *JHEP* **07**, 063, arXiv:0812.0354 [hep-th].
- [24] A. D. Martin, W. J. Stirling, R. S. Thorne, and G. Watt, *Eur. Phys. J. C* **63**, 189 (2009), arXiv:0901.0002 [hep-ph].
- [25] M. Hirai, S. Kumano, and N. Saito, *Phys. Rev. D* **74**, 014015 (2006), arXiv:hep-ph/0603213.
- [26] R. Nishio and T. Watari, *Phys. Rev. D* **90**, 125001 (2014).
- [27] S. Bhattacharya *et al.*, *Phys. Rev. D* **109**, 034508 (2024), arXiv:2310.13114 [hep-lat].
- [28] G. Basar, D. E. Kharzeev, H.-U. Yee, and I. Zahed, *Phys. Rev. D* **85**, 105005 (2012), arXiv:1202.0831 [hep-th].
- [29] K. A. Mamo and I. Zahed, *Phys. Rev. D* **108**, 086026 (2023), arXiv:2206.03813 [hep-ph].
- [30] O. V. Teryaev, (1999), arXiv:hep-ph/9904376.
- [31] Y. Liu and I. Zahed, *Phys. Rev. D* **100**, 046005 (2019), arXiv:1803.09157 [hep-ph].
- [32] C. Lorcé, *Phys. Lett. B* **735**, 344 (2014), arXiv:1401.7784 [hep-ph].
- [33] C. Alexandrou, S. Bacchio, M. Constantinou, J. Finkenrath, K. Hadjiyiannakou, K. Jansen, G. Koutsou, H. Panagopoulos, and G. Spanoudes, *Phys. Rev. D* **101**, 094513 (2020), arXiv:2003.08486 [hep-lat].
- [34] J. Liang, Y.-B. Yang, T. Draper, M. Gong, and K.-F. Liu, *Phys. Rev. D* **98**, 074505 (2018), arXiv:1806.08366 [hep-ph].
- [35] J. Green, N. Hasan, S. Meinel, M. Engelhardt, S. Krieg, J. Laeuchli, J. Negele, K. Orginos, A. Pochinsky, and S. Syritsyn, *Phys. Rev. D* **95**, 114502 (2017), arXiv:1703.06703 [hep-lat].

END MATTER

Derivation of Eq. (7).— Starting from the Hankel representation of the type

$$\rho_n^{\mathcal{H}_a}(b_\perp; \eta) = \frac{1}{2\pi} \int_0^\infty dq q J_0(qb_\perp) \mathcal{H}_a(q^2 + c_\eta, \eta), \quad (\text{S1})$$

the plane integral reads

$$N_n^{\mathcal{H}_a}(\eta) = 2\pi \int_0^\infty b_\perp db_\perp \rho_n^{\mathcal{H}_a}(b_\perp; \eta). \quad (\text{S2})$$

Exchanging integrations and using $\int_0^\infty b db J_0(qb) = \delta(q)/q$ we obtain

$$N_n^{\mathcal{H}_a}(\eta) = \int_0^\infty dq q \mathcal{H}_a(q^2 + c_\eta, \eta) \frac{\delta(q)}{q} = \mathcal{H}_a(c_\eta, \eta). \quad (\text{S3})$$

Because the integrand in Eq.(5) depends only on $\Delta_\perp = |\mathbf{\Delta}_\perp|$, the Fourier integral separates into two cylindrically symmetric Hankel transforms

$$\rho_n^{\mathcal{H}_a}(b_\perp; \eta) = \frac{1}{2\pi} \int_0^\infty d\Delta_\perp \Delta_\perp J_0(\Delta_\perp b_\perp) \mathcal{H}_a(n, \eta, t), \quad (\text{S4a})$$

$$\rho_n^{\mathcal{E}_a}(b_\perp; \eta) = \frac{1}{2\pi} \int_0^\infty d\Delta_\perp \Delta_\perp^2 J_1(\Delta_\perp b_\perp) \mathcal{E}_a(n, \eta, t), \quad (\text{S4b})$$

where

$$\begin{aligned} \mathcal{H}_a(n, \eta, t) &\equiv \mathbb{H}_a^{(\pm)} \left(n, \eta, -\frac{\Delta_\perp^2}{1-\eta^2} - c_\eta \right), \\ \mathcal{E}_a(n, \eta, t) &\equiv \mathbb{E}_a^{(\pm)} \left(n, \eta, -\frac{\Delta_\perp^2}{1-\eta^2} - c_\eta \right). \end{aligned}$$

Therefore, the full density decomposes into

$$\rho_n^a(\mathbf{b}_\perp; \eta) = \rho_n^{\mathcal{H}_a}(b_\perp; \eta) + \frac{b_y}{2m_N b_\perp} \rho_n^{\mathcal{E}_a}(b_\perp; \eta). \quad (\text{S5})$$

The full strength of the string–nucleon correlation is obtained by integrating the complete density (S5) over the transverse plane

$$\begin{aligned} N_n^a(\eta) &= \int d^2 b_\perp \rho_n^a(\mathbf{b}_\perp; \eta) = \int d^2 b_\perp \rho_n^{\mathcal{H}_a}(b_\perp; \eta) \\ &\quad + \frac{1}{2m_N} \int d^2 b_\perp \frac{b_y}{b_\perp} \rho_n^{\mathcal{E}_a}(b_\perp; \eta). \end{aligned} \quad (\text{S6})$$

The second term vanishes identically: in polar coordinates $b_y = b_\perp \sin \theta$ and the angular integral $\int_0^{2\pi} d\theta \sin \theta =$

0 cancels the entire helicity-flip contribution. Hence, only the spin-conserving part survives

$$N_n^a(\eta) = \int d^2 b_\perp \rho_n^{\mathcal{H}_a}(b_\perp; \eta) = \mathcal{H}_a(c_\eta, \eta), \quad (\text{S7})$$

TABLE S1: Open- and closed-string slopes (GeV^{-2}) entering Eq. (2). A dash denotes that no secondary trajectory is required.

Channel	α'_{u-d}	α'_{u+d}	α'_{u+d}^{S}	α'_g	α'_g^{S}
$\mathbb{H}^{(\pm)}$	0.66	0.96	1.83	0.63	4.28
$\mathbb{E}^{(\pm)}$	1.48	1.12	–	–	–
$\tilde{\mathbb{H}}^{(\pm)}$	0.45	0.30	1.18	0.49	0.74

which is Eq. (7) of the main text.

Nucleon spin decomposition at finite skewness.— We write the total angular–momentum form factor as a sum of quark and gluon contributions $\mathcal{J}^z(\eta, t) = \sum_{a=q,g} \mathcal{J}_a^z(\eta, t)$ with individual terms

$$\mathcal{J}_a^z(\eta, t) = \frac{1}{2} [\mathbb{H}_a^{(+)}(2, \eta, t) + \mathbb{E}_a^{(+)}(2, \eta, t)]. \quad (\text{S8})$$

Following Ji's decomposition [2], the quark or gluon spin (helicity) contribution is $S_a^z(\eta, t) = \frac{1}{2} \tilde{\mathbb{H}}_a^{(+)}(1, \eta, t)$ while the orbital part is obtained by subtraction:

$$\begin{aligned} L_a^z(\eta, t) &= \mathcal{J}_a^z(\eta, t) - S_a^z(\eta, t) \\ &= \frac{1}{2} [\mathbb{H}_a^{(+)}(2, \eta, t) + \mathbb{E}_a^{(+)}(2, \eta, t)] - \frac{1}{2} \tilde{\mathbb{H}}_a^{(+)}(1, \eta, t). \end{aligned} \quad (\text{S9})$$

The spin–orbit correlation introduced in Ref. [32] is, in the present notation,

$$C_a^z(\eta, t) = \frac{1}{2} [\tilde{\mathbb{H}}_a^{(-)}(2, \eta, t) - \mathbb{H}_a^{(-)}(1, \eta, t)]. \quad (\text{S10})$$

These expressions are used to derive the results in Tables S2 ($t = 0, \eta = 0$) and to generate Fig. 1. Note that, throughout this Letter, the unpolarized \mathbb{H}_a conformal moments and H_a GPDs at $\mu = \mu_0 = 1 \text{ GeV}$ are taken from [13, 14] after evolving them to $\mu = 2 \text{ GeV}$ at NLO.

Spin tomography at $\eta = 0$.— In Fig. S1 we provide the impact-parameter representation of the orbital angular momentum and spin–orbit correlations in the nucleon at $\eta = 0$

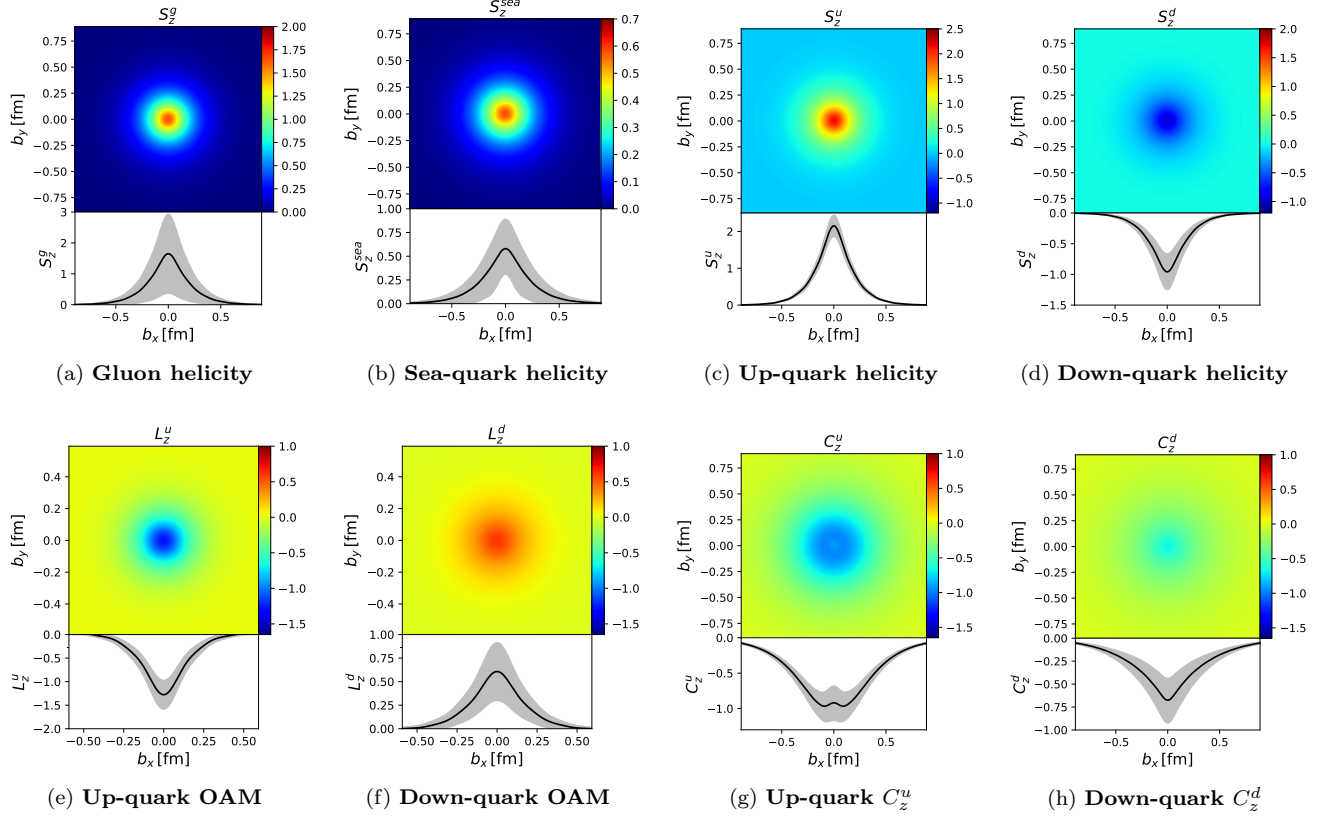


FIG. S1: Impact-parameter distributions for helicity densities (top row) and orbital angular momentum and spin-orbit correlations (bottom row) at $\mu = 2$ GeV and $\eta = 0$ in the nucleon.

(a) $\mu = 2$ GeV (NLO evolved)					
	<i>u</i>	<i>d</i>	<i>s</i>	<i>g</i>	total
S_z (this work)	0.421(66)	-0.210(66)	-0.039(194)	0.372(330)	0.544(394)
S_z [33]	0.432(8)	-0.213(8)	-0.023(4)	—	—
S_z [34]	0.424(18)	-0.204(12)	-0.018(4)	—	—
S_z [35]	0.432(7)	-0.173(54)	-0.012(12)	—	—
L_z (this work)	-0.082(86)	0.071(86)	0.147(217)	-0.179(340)	-0.044(421)
\mathcal{J}_z (this work)	0.339(110)	-0.139(110)	0.108(291)	0.192(474)	0.50(57)
(b) $\mu = 1$ GeV (input scale)					
	<i>u</i>	<i>d</i>	<i>s</i>	<i>g</i>	total
S_z (this work)	0.421(66)	-0.210(66)	-0.027(185)	0.156(185)	0.341(280)
L_z (this work)	-0.071(86)	0.066(86)	0.141(210)	0.023(206)	0.159(318)
\mathcal{J}_z (this work)	0.350(110)	-0.143(110)	0.114(280)	0.179(279)	0.50(42)

TABLE S2: Proton spin decomposition at $t = 0$ and $\eta = 0$ for two renormalization scales. Statistical uncertainties are shown in parentheses; “—” denotes values not quoted in the cited works.